



## Article

## Carbon and Energy Balance in a Primary Amazonian Forest and Its Relationship with Remote Sensing Estimates

Mailson P. Alves <sup>1,2</sup>, Rommel B. C. da Silva <sup>3</sup>, Cláudio M. Santos e Silva <sup>1,2,4</sup> , Bergson G. Bezerra <sup>1,2</sup>, Keila Rêgo Mendes <sup>1,2</sup>, Larice A. Marinho <sup>1</sup>, Melahel L. Barbosa <sup>1,5</sup>, Hildo Giuseppe Garcia Caldas Nunes <sup>1,6</sup> , José Guilherme Martins Dos Santos <sup>1,7</sup> , Theomar Trindade de Araújo Tiburtino Neves <sup>1,5</sup>, Raoni A. Santana <sup>1,5</sup>, Lucas Vaz Peres <sup>1,5</sup>, Alex Santos da Silva <sup>1,5</sup>, Petia Oliveira <sup>1,8</sup>, Victor Hugo Pereira Moutinho <sup>1,9</sup> , Wilderclay B. Machado <sup>1,5</sup> , Iolanda M. S. Reis <sup>1,9</sup>, Marcos Cesar da Rocha Seruffo <sup>1,10</sup> , Avner Brasileiro dos Santos Gaspar <sup>1,9</sup>, Waldeir Pereira <sup>1,11</sup> and Gabriel Brito-Costa <sup>1,2,8,9,10,11,12,\*</sup>

- <sup>1</sup> Research Group Interaction Biosphere-Atmosphere and Micrometeorology on Amazonia (IBAMA), Federal University of Western Pará (UFOPA), Santarém 68040-255, Brazil
- <sup>2</sup> Climate Sciences Post-Graduate Program (PPGCC), Federal University of Rio Grande do Norte, Av. Senador Salgado Filho, 3000, Natal 59078-970, Brazil
- <sup>3</sup> Large Biosphere Atmosphere in Amazon Program, LBA/INPA, 1901, Belém 66077-830, Brazil
- <sup>4</sup> Institute of Geosciences, PPG-Environmental Sciences, Federal University of Pará, Belém 66075-110, Brazil
- <sup>5</sup> Institute of Engineering and Geosciences, Federal University of West Pará, Rua Vera Paz s/n, Salé, Santarém 68040-255, Brazil
- <sup>6</sup> Socio-Environmental and Water Resources, Federal Rural University of the Amazon, Belém 66077-830, Brazil
- <sup>7</sup> Wildfire Monitoring Program, National Institute for Space Research, São José dos Campos 12227-010, Brazil
- <sup>8</sup> Post-Graduate Program in Natural Resources of the Amazon—PPGRNA, Federal University of Western Pará (UFOPA), Santarém 68035-110, Brazil
- <sup>9</sup> Institute of Biodiversity and Forests, Federal University of West Pará, Rua Vera Paz s/n, Santarém 68040-255, Brazil
- <sup>10</sup> Anthropoc Studies in the Amazon Post-Graduate Program (PPGEAA), Federal University of Pará, Castanhal 68740-222, Brazil
- <sup>11</sup> Biosciences Post-Graduate Program (PPGBIO), Federal University of Western Pará (UFOPA), Santarém 68035-110, Brazil
- <sup>12</sup> Biotechnology and Biodiversity—Bionorte Network, Federal University of Pará, Rua Augusto Corrêa, 01, Guamá, Belém 66075-900, Brazil
- \* Correspondence: gabriel.costa@ufopa.edu.br



**Citation:** Alves, M.P.; da Silva, R.B.C.; Silva, C.M.S.e.; Bezerra, B.G.; Rêgo Mendes, K.; Marinho, L.A.; Barbosa, M.L.; Nunes, H.G.G.C.; Dos Santos, J.G.M.; Neves, T.T.d.A.T.; et al. Carbon and Energy Balance in a Primary Amazonian Forest and Its Relationship with Remote Sensing Estimates. *Remote Sens.* **2024**, *16*, 3606. <https://doi.org/10.3390/rs16193606>

Academic Editors: Celso Augusto Guimarães Santos, Prashant Srivastava, Harry West, Nevil Quinn, Shaeden Gokool and Michael Horswell

Received: 28 July 2024

Revised: 17 September 2024

Accepted: 25 September 2024

Published: 27 September 2024



**Copyright:** © 2024 by the authors. Licensee MDPI, Basel, Switzerland. This article is an open access article distributed under the terms and conditions of the Creative Commons Attribution (CC BY) license (<https://creativecommons.org/licenses/by/4.0/>).

**Abstract:** With few measurement sites and a great need to validate satellite data to characterize the exchange of energy and carbon fluxes in tropical forest areas, quantified by the Net Ecosystem Exchange (NEE) and associated with phenological measurements, there is an increasing need for studies aimed at characterizing the Amazonian environment in its biosphere–atmosphere interaction, considering the accelerated deforestation in recent years. Using data from a flux measurement tower in the Caxiuanã-PA forest (2005–2008), climatic data, CO<sub>2</sub> exchange estimated by eddy covariance, as well as Gross Primary Productivity (GPP) data and satellite vegetation indices (from MODIS), this work aimed to describe the site’s energy, climatic and carbon cycle flux patterns, correlating its gross primary productivity with satellite vegetation indices. The results found were: (1) marked seasonality of climatic variables and energy flows, with evapotranspiration and air temperature on the site following the annual march of solar radiation and precipitation; (2) energy fluxes in phase and dependent on available energy; (3) the site as a carbon sink ( $-569.7 \pm 444.9 \text{ gC m}^{-2} \text{ year}^{-1}$ ), with intensity varying according to the site’s annual water availability; (4) low correlation between productivity data and vegetation indices, corroborating data in the literature on these variables in this type of ecosystem. The results show the importance of preserving this type of environment for the mitigation of global warming and the need to improve satellite estimates for this region. NDVI and EVI patterns follow radiative availability, as does LAI, but without direct capture related to GPP data, which correlates better with satellite data only in the months with the highest LAI. The results show the significant difference at a point measurement to a satellite interpolation, presenting how important preserving any type of environment is, even related to its size, for the global climate balance, and also the need to improve satellite estimates for smaller areas.

**Keywords:** eddy covariance; enhanced vegetation index; gross primary production; normalized vegetation index

## 1. Introduction

Many studies on carbon and water exchange have been carried out in different biomes in South America, such as the Caatinga [1–7], grazed pasture [8,9], Pantanal [10,11], Cerrado [12,13], and the Amazon, which probably concentrates most of the studies [14–18], in addition to integrated analyses of the biomes [19–21]. Understanding the seasonality of exchanges and the resistance and adaptability of species to increasingly frequent water stresses [22] is of the utmost importance in studies on biosphere–atmosphere interaction with a focus on South America, especially the Amazon biome, in addition to environmental studies [23–25] to characterize the impacts of environmental changes on soil properties.

The Amazon Basin is at the center of increasingly intense discussions on deforestation, land use and global change, such as studies on carbon (C) cycling and storage and its implications for the global climate [26], as well as factors that affect the quality of life of the population [15]. Forests like this harbor around 10 to 15% of the Earth's biodiversity, and have abundant rainfall of around 2200 mm/year, which makes the region an important source of heat and humidity for the atmosphere and generates an estimated 210,000 m<sup>3</sup>/s to 220,000 m<sup>3</sup>/s of river flow, which is ~15% of the freshwater inflow into the oceans. In addition, it stores around 150 to 200 billion tons of carbon and presents a mosaic of ethnological and linguistic diversity [27]. An increasing number of studies [28–30] are aimed at characterizing forest environments in terms of their soil, atmosphere and water characteristics and properties and their contributions to greenhouse gas emissions and climate change mitigation, particularly in Brazil's Amazon region.

Given its significance, studies on Amazonia related to water, carbon and nutrient cycles, as well as solar energy balances, as a result of changes in the region's vegetation cover, are frequently carried out by researchers from the Large Scale Biosphere–Atmosphere Program in the Amazon (LBA). Wofsy et al. [31] showed that high CO<sub>2</sub> concentrations in the early morning occur due to ecosystem respiration in a stable nocturnal atmospheric layer, and some previous studies point to the Amazon rainforest as a potential sink for atmospheric CO<sub>2</sub> [32–34] with micrometeorological measurements via flux towers.

Previous studies have indicated seasonal patterns in gross primary production (GPP), ecosystem respiration (RECO), net ecosystem exchange (NEE), energy exchange, phenology and tree growth [35–38], and they usually found that the seasonal course of canopy photosynthesis was largely controlled by phenology and light. GPP refers to the total amount of carbon fixed by plants in an ecosystem through the process of photosynthesis, and it is an important component of the carbon balance that has been analyzed in studies since the 2000s, whereas carbon cycle studies seek to support tower measurements with data from biometric or satellite measurements [35–38].

Saleska et al. [36] compared micrometeorological estimates and biometric measurements in Santarém-PA, and they reported a CO<sub>2</sub> source to the atmosphere of 1.3 Mg C ha<sup>−1</sup> year<sup>−1</sup> associated with the prevalence of emissions from the decomposition of necromass in previous episodes of high tree mortality in the region. Miller et al. [37] reported slightly positive ecosystem fluxes (considering NEE > 0 = source, NEE < 0 = sink) of 0.4 Mg C ha<sup>−1</sup> year<sup>−1</sup> corroborated by biometric measurements. Espírito Santo et al. [38] combined satellite estimates and field data to suggest that uptake by living trees exceeds emission by dead trees, reinforcing evidence of terra firme forest acting as a carbon sink in aerial biomass.

There has been an increase in the number of studies using remote sensing data [39–41] to characterize environmental variables in large areas, sometimes with a very low density of in situ data. Validation of this information is required to increase the security of the information generated and to have confidence in the public policies and mitigating actions to be taken based on these data. This information is important for studies on forest

biomass [42,43] and other applications [44–46], and although it has good accuracy and validation in some regions, it still requires validation in many remote areas, such as the MODIS products for the Amazon.

The Moderate Resolution Imaging Spectroradiometer (MODIS) remote sensing data suggest that photosynthesis in native forests increases as the dry season progresses over a large area of central Amazonia. The MODIS Leaf Area Index (LAI) product shows a pattern of increase during the dry season, peaking at the beginning and in the middle of the dry season [47]. Similarly, the MODIS Enhanced Vegetation Index (EVI) shows that the equatorial forests of Amazonia continue to “green up” throughout the dry season as the availability of sunlight increases [48]. Costa et al. [20] showed that the seasonality of GPP measurements and flux tower data have different associations and correlations throughout the year depending on the type of forest, with data being better correlated in certain months of the year and in certain locations, which would make it easier to extrapolate the analysis to a large area with satellite data.

Considering the above, it is important to conduct more studies aimed at characterizing the CO<sub>2</sub> exchange environment in areas of the Amazon rainforest with the atmosphere and its relationship with vegetation indices estimated by satellite. Despite many studies on the subject in recent years [16,49,50], the Caxiuanã region still lacks research into these estimates for longer periods of its data series and with analyses integrated with satellite data, which are important due to the diverse mosaic of natural environments within the Amazon biome. There are particularities in the exchange of water and CO<sub>2</sub> with the atmosphere in the Amazon basin, and there may be areas that are sinks, neutral, or even sources of CO<sub>2</sub> for the atmosphere, especially in the context of climate change and the influence of severe droughts caused by low-frequency phenomena such as ENOS (El Niño Southern Oscillation).

It is known that GPP data from eddy covariance towers are not representative of the global distribution of ecosystem types [51,52], increasing the need for remote sensing approaches to estimate GPP that can provide information on ecosystem dynamics in response to climate variability at both the regional and global scales [52]. As not all environments within the same biome show the same correlations between surface data and satellite data, it is important that more studies perform this survey to validate this information and help improve or adjust estimates where it is not yet efficient.

This creates the necessity to understand these cycles, their controls and their influences, which is the purpose of this study, which aims to: (1) characterize diurnal and daily variations in energy and CO<sub>2</sub> fluxes in the Caxiuanã forest (Rn, H, LE, NEE); (2) quantify the CO<sub>2</sub> flux (g C m<sup>−2</sup> d<sup>−1</sup>) using metrics including gross primary production (GPP), ecosystem respiration (Reco) and NEE measurements; and (3) analyze the patterns and correlations of the site’s gross primary productivity with vegetation indices (NDVI, EVI and LAI from MODIS satellite) and other satellite estimates.

## 2. Materials and Methods

### 2.1. Description of the Experimental Area

The site is located inside the Caxiuanã National Forest (latitude 01°42′30″S and longitude 51°31′45″W), at Melgaço city, state of Para, about 250 km west of the capital, Belém (Figure 1). About 85% of its area is formed by dense land forest, with a median height of 30 m; however, certain trees reach 50 m [53]. The location is part of the Ferreira Pena Scientific Station (ECFPn). According to Köppen’s classification [54], the region’s climate is tropical hot and humid, with minimum, average and maximum annual temperatures equal to 22, 26 and 32 °C, respectively. The rainy season in the region is from December to May, and the dry season is from June to November [55]. According to Souza Filho et al. [56], the radiation balance in the forest is lower in the rainy period compared to the dry period, a factor that can be explained by the higher solar irradiance in the dry period, due to less cloudiness in this period.

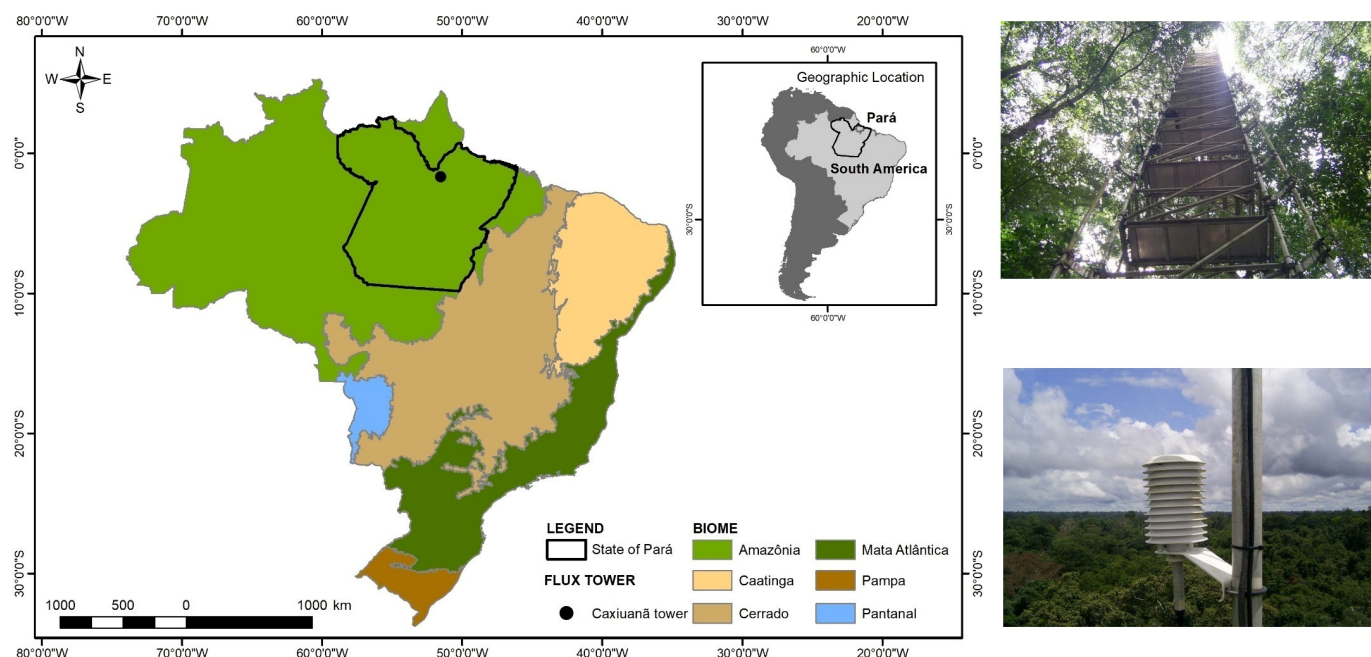


**Figure 1.** Location of the micrometeorological tower in the Caxiuanã-PA forest, with a view of the base of the installed tower and the temperature and humidity sensor at the top of the tower.

## 2.2. Database

The database of meteorological, energy and CO<sub>2</sub> fluxes, as well as satellite data, covers the period from 1 January 2005 to 31 December 2008. The data analyzed in this study were collected from an automatic weather station (Table 1) belonging to the Large Scale Biosphere–Atmosphere Program (LBA), installed in a 52 m-high micrometeorological observation tower. Precipitation (PRP) was measured by a Campbell TB3/TB4 (CS700, Campbell Scientific, Leicester, UK) rain gauge. Air temperature (Tar) measurements were obtained using Campbell’s HMP45 AC device (Campbell Scientific, Leicester, UK). The GPP was estimated from CO<sub>2</sub> flux data measured in situ, following the methodology of Huttyra et al. [57], with eddy covariance data measured from a Licor 7500 Open Path CO<sub>2</sub>/H<sub>2</sub>O Analyzer (LICOR, Lincoln, NE, USA), which works in conjunction with a Gill instruments 3D input unic sonic anemometer (Solent, Gill Instruments, Lymington, UK).

**Table 1.** List of variables, measuring instruments and measuring units involved in the study (Source: LBA project and NASA).

Measurements/Sampling Rate/Averaging Period/Spatial Resolution	Data Source
Direction (°) and Wind Speed (m/s); Eddy Covariance: Turbulent Fluxes of Latent Heat (W m <sup>-2</sup> ), Sensible Heat (W m <sup>-2</sup> ) and CO <sub>2</sub> (μmol m <sup>-2</sup> s <sup>-1</sup> )/5 Hz/30 min/55 m.	Three-dimensional sonic anemometer (Solent, Gill Instruments, Lymington, UK); Li-7500 infrared gas analyzer (LICOR, Lincoln, NE, USA)
Incident and Reflected Photosynthetically Active Radiation (μmol m <sup>-2</sup> s <sup>-1</sup> )/1 min/30 min/52 m.	Skye quantum sensor (Skye Instruments, Powys, UK)
Radiation Balance (W m <sup>-2</sup> )/1 min/30 min/45.5 m.	1 radiometer balance (CNR1, Kipp & Zonen, Delft, The Netherlands)
Temperature (°C) and Relative Humidity (%)/1 min/30 min/53 m.	HMP45 AC (Campbell Scientific, Leicester, UK)
Rainfall (mm)/1 min/30 min/53 m.	Bucket rainfall gauge (CS700, Campbell Scientific, Loughborough, UK)
MODIS GPP (g C m <sup>-2</sup> day <sup>-1</sup> )/8 days/500 m. (mean in 8 days)	MOD17A2H-MODIS/Terra Gross Primary Productivity
NDVI and EVI/16 days/250 m. (mean in 16 days)	MOD13Q1-MODIS/Terra Vegetation Indices
LAI/8 days/500 m. (mean in 8 days)	MCD15A2H-MODIS/Terra + Aqua

All the inherent corrections of the eddy covariance method (such as coordinate rotation correction using the planar fit method, sonic virtual temperature correction, corrections for



density fluctuation (WPL-correction), and frequency response correction) for estimating energy and CO<sub>2</sub> fluxes, the complete instrumentation of the tower, and the gap filling method for missing data are described in previous publications [1,49,55,57]. The information generated from the gas analyzer/sonic anemometer set was used to determine the flows and concentration of CO<sub>2</sub> at the ecosystem level, and this information was recorded on a data storage device (iPAQ). The evapotranspiration (ET) of the site was estimated using latent heat (Equation (1) [7]):

$$ET = 86,400 \cdot \frac{LE}{L} \quad (1)$$

where  $L$  ( $\text{J kg}^{-1}$ ) =  $103 \times (2500 - 2.37 \times T_a)$ ,  $LE$  is the latent heat flux, and 86,400 is the daily integration factor. The flux density of an atmospheric variable is estimated on the concept that the turbulent flow of this magnitude is calculated by its covariance with the vertical component of the wind speed. In the case of turbulent CO<sub>2</sub> fluxes ( $F_c$ ), sensible heat flux ( $H$ ) and latent heat flux ( $LE$ ) can be written as [58]

$$F_c = \overline{w' \rho_c'} \quad (2)$$

$$H = \rho c_p \overline{w' T'} \quad (3)$$

$$LE = \rho L \overline{w' q'} \quad (4)$$

where  $w'$ ,  $\rho_c'$ ,  $T'$  and  $q'$  are the fluctuations of the average over a time interval (usually 30 min) of the vertical wind component, CO<sub>2</sub> density, air temperature and air specific humidity, respectively.  $L$  is the latent heat of vaporization,  $\rho$  is the air density, and  $c_p$  is the specific heat of air at constant pressure. The NEE is calculated from the total amount of turbulent flux ( $F_c$ ) and the storage term ( $St$ ).  $St$  is the flux associated with the CO<sub>2</sub> stored in the layer below the level at which the CO<sub>2</sub> flux measurements are made. The value of  $St$  is obtained by integrating the variation of the CO<sub>2</sub> concentration in the air in the layer up to the eddy covariance height. Carswell et al. [16] showed that night respiration and daytime photosynthesis eventually compensate for each other in terms of storage for the studied site, so it is possible to assume that  $F_c \sim \text{NEE}$ . GPP is the difference between estimated ecosystem respiration (Reco) and observed NEE:

$$GPP = \text{Reco} - \text{NEE} \quad (5)$$

Reco are the averages of the nocturnal (19–06 h) CO<sub>2</sub> flux data. The vapor pressure deficit data was estimated according to Campos et al. [2] in 30-min averages. A net radiometer measured radiation net (Rn) with incoming and reflected solar and longwave radiation (CNR1, Kipp & Zonen, Delft, The Netherlands).

### 2.3. Remote Sensing Products

Vegetation indices play an important role in monitoring agricultural crops and vegetated surfaces using multispectral satellite imagery or other technologies. Several sensors can be used to obtain vegetation indices, but the most widely used are the Normalized Difference Vegetation Index (NDVI), which is used to monitor surface growth and vegetative vigor [59], and the Enhanced Vegetation Index (EVI), which uses the red and infrared bands like NDVI, but uses the blue band to remove atmospheric influences [59].

To access the seasonality of phenology on site, the x NDVI was used, which presents the direct relationship with leaf chlorophyll content, i.e., the higher the index, the more new leaves (leaf flush) in the canopy. The time series of surface reflectance from the MODIS sensor (on board the Terra and Aqua satellites) with atmospheric correction from the MAIAC algorithm (multi-angle implementation of atmospheric correction) have 1 km of

spatial resolution and are temporally aggregated in 16-day compositions. These images are used to calculate the Normalized Vegetation Index (NDVI) described in Equation (6):

$$NDVI = \rho_{NIR} - \rho_{Red} / \rho_{NIR} + \rho_{Red} \quad (6)$$

where NIR is near-infrared (841–876 nm) and Red is red band (620–670 nm). These wavelength values refer to the MODIS product. For the estimation of the leaf area index (LAI), the product MCD15A3H (v006)—Terra + Aqua LAI was used, which consists of the composition of 4 days in the selection of best data values in the selected period by two satellites, according to Myneni et al. [60]. However, the EVI decouples soil and atmosphere influences from the vegetation response by correcting the  $\rho_{NIR}/\rho_{red}$  ratio using visible blue reflectance ( $\rho_{blue}$ ) and correction coefficients [61]:

$$EVI = 2.5 \left( \frac{\rho_{NIR} - \rho_{red}}{\rho_{NIR} + 6\rho_{red} - 7.5\rho_{blue} + 1} \right) \quad (7)$$

#### 2.4. MOD15 and MOD17 Products

The Leaf Area Index (LAI), one of the six layers of the MOD15 product, was used to evaluate the relationship between satellite data and surface phenological patterns. The MOD15 algorithm uses daily surface reflectance values (MOD09) and data from a radiative transfer model, which are stored in a two-dimensional Lookup Table (LUT) [62]. MOD17 contains three layers, corresponding to gross primary production (GPP), net photosynthesis (PSnet) and PSnet pixel quality, with a 500 m spatial resolution. GPP is calculated on a daily scale, but the products are available with the sum for an 8-day period. The GPP derived from the MOD17 algorithm (GPPmod) is based on the linear relationship between absorbed photosynthetically active radiation and light use efficiency (LUE) [63] and is obtained according to Equation (8).

$$GPP = \varepsilon \times APAR \quad (8)$$

where  $\varepsilon$  is the light use efficiency (LUE) and APAR is the absorbed photosynthetically active radiation. Although there are a large number of satellite environmental data measurement platforms [64,65], the MODIS data were chosen because of the ease of NASA's specific data site tool, which provides various satellite information for these and other land measurement points, with varied environmental information available at: [https://modis.ornl.gov/sites/?id=br\\_para\\_caxiuana\\_forest\\_almeirim#product\\_table](https://modis.ornl.gov/sites/?id=br_para_caxiuana_forest_almeirim#product_table), accessed on 25 January 2023.

The NDVI and EVI data are averaged every 16 days, while LAI values are estimated every 8 days. In order to compare them with other variables, they were averaged over the same period as the NDVI, EVI and LAI values.

#### 2.5. Data Quality Control and Outlier Detection

Data post-processing was conducted in three stages: (i) data quality assessment, rejecting low-quality data, data associated with sensor malfunction and visibly inconsistent data; (ii) the data were subjected to a robust outlier detection algorithm, as proposed in the literature [15]; and (iii) due to the low turbulence conditions at night, all night flow data were rejected if the friction velocity ( $u^*$ ) was below a critical threshold (m/s); (iv) due to the low turbulence conditions at night, all night flow data were rejected if the friction velocity ( $u^*$ ) was below a critical threshold (0.22 m/s) according to the method suggested in the literature [17,66].

The estimation of the  $u^*$ -threshold was based on the moving point test (MPT) algorithm on nighttime data, as described by the literature [67]. To eliminate spurious oscillations in the  $CO_2$  and energy fluxes values, an algorithm based on median analysis (moving median) was used to identify spurious oscillations. The method consists of separating the series of values into a smooth part and a residual part, after which the discrepant values are manually removed.

The gaps arising from the exclusion of spurious data during the screening process were filled using the marginal distribution sampling (MDS) gap-filling algorithm, which takes into account the covariation of fluxes with meteorological variables and also the temporal auto-correlation of fluxes [68]. In this algorithm, actions are taken under the following conditions: (i) if flow data are missing but meteorological data are available (air temperature and vapor pressure deficit—VPD), the gap is filled with the average value considering similar meteorological conditions in a 7-day window; (ii) if only incident solar radiation data are available, the gap is filled with the average value considering similar meteorological conditions in a 7-day window; (iii) if no meteorological data are available, the gap is filled with the average value of the last hour, thus considering the diurnal variation of each variable. If there are still data gaps after applying the algorithm, the same procedures are performed but consider longer time windows. The gap-filling method was performed using an online tool from the Max Planck Institute for Biogeochemistry (<http://www.bgc-jena.mpg.de/~MDIwork/eddyproc/>, accessed on 27 January 2023).

The hyperbolic relationship pattern (Michaelis–Menten model) between NEE and photosynthetically active radiation (PAR, or photosynthetic photon flux density (PPFD)) involves coefficients that represent the maximum photosynthetic efficiency of the canopy ( $a_2$ ), its yield ( $a_3$ ) and the average nocturnal respiration of the ecosystem ( $a_1$ ) as the intercept of the curve [17], and this allows for the correction of NEE daytime data failures, such that:

$$NEE = a_1 + (a^2 \times PAR / a^3 + PAR) \quad (9)$$

### 3. Results

#### 3.1. Climate Variables and Energy Fluxes

In carbon cycle characterization work, a complete and in-depth description of local atmospheric patterns is required, which are usually the main controls on site productivity variability. The study site showed marked seasonality in terms of rainfall and air temperature (Figure 2), with more intense precipitation events (rainy days) during the region's rainy season (December to May) and less intense events during the dry season (June to November). The large number of intense rainfall events causes the highest density of daily air temperature averages to be below 25 °C in the months of February and March, and the greatest variability of air temperature occurs at the end of the rainy season, with temperatures between 18 and 27.5 °C, in the month of May.

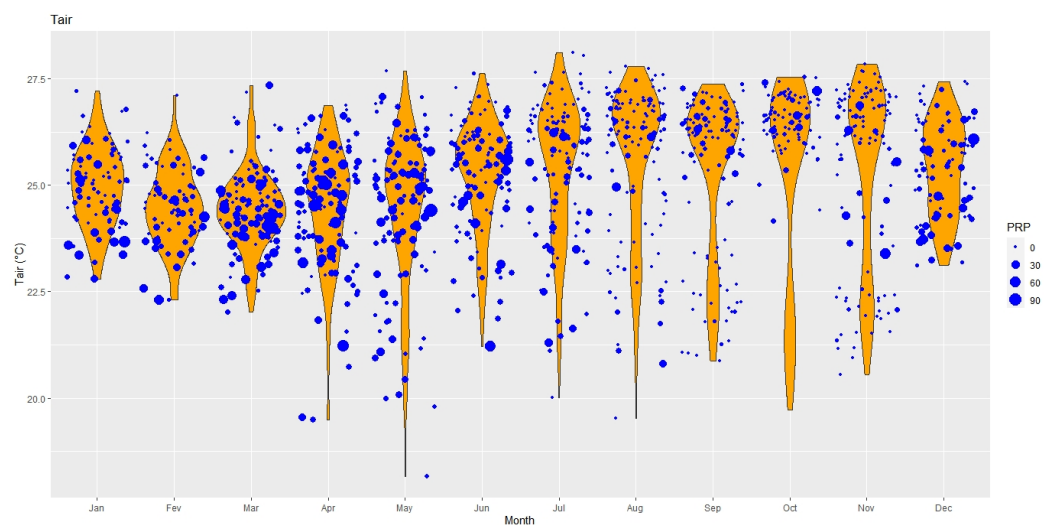


**Figure 2.** Data density distribution of monthly air temperature (°C) by precipitation intensity (mm/day) in Caxiuanã-PA.

The wind circulation patterns are shown in Figure 3. Throughout the year, the highest frequency of wind direction is from the NE–E quadrants, with more than 40% of the local

wind coming from the NE direction in October. The highest average speed occurred in December (1.9 m/s), and the lowest average speed occurred in April (1.4 m/s). Wind speed tended to increase (highest averages and highest occurrences in the 2–4 and 4–6 m/s ranges) between June and December, which marks the beginning of the dry season and the start of the rainy season, with a tendency for speed to decrease from January onwards.

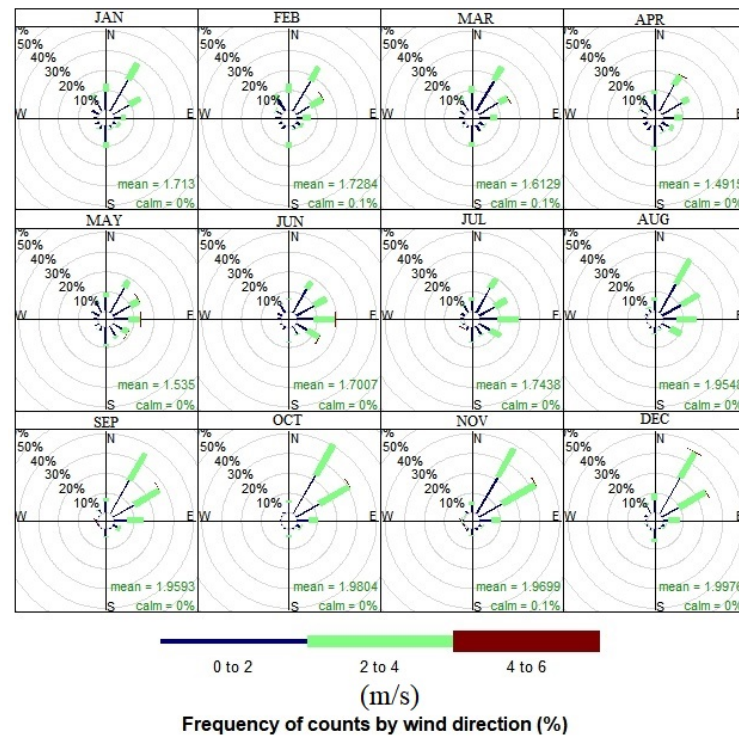


**Figure 3.** Annual wind patterns at the Caxiuanã site.

Monthly temperature averages tend to decrease continuously from December until reaching their minimum value in May (Figure 4a) and from this month onwards, with an increasing trend until August, coinciding with the maximum photosynthetically active radiation (Figure 4c). The maximum evapotranspiration occurs in September (Figure 4b), the same period in which the minimum rainfall occurs (Figure 4d), with the highest rainfall in April (around 400 mm). The statistical summary of the data by season is presented in Table 2.

**Table 2.** Seasonal midday average of meteorological variables, carbon variables and energy balance components. GPP is from the eddy covariance method. Rainfall and ET are accumulated for each period; EVI and NDVI are 16-day averages.

Variable	Dry Season			Wet Season		
	Mean	Sd	Max	Mean	Sd	Max
T <sub>air</sub> (°C)	27.3	±3.0	31.9	23.3	±1.6	35.31
PPFD (μmol m <sup>−2</sup> s <sup>−1</sup> )	772.5	±391.0	1667.5	9.1	±70.6	1391.9
Rainfall (mm)	3.3	±8.2	77.7	10.2	±14.7	113.4
ET (mm)	1.5	±0.46	3.0	1.2	±0.56	2.5
R <sub>n</sub> (W m <sup>−2</sup> )	328.1	±208.6	802.0	12.0	±24.1	151.2
LE (W m <sup>−2</sup> )	202.0	±132.9	745.0	5.1	±11.7	160.1
H (W m <sup>−2</sup> )	67.7	±58.7	417.9	12.4	±11.6	267.9
NDVI	0.83	±0.02	0.88	0.80	±0.04	0.86
EVI	0.51	±0.07	0.64	0.46	±0.07	0.70
GPP (μmol m <sup>−2</sup> s <sup>−1</sup> )	12.4	±3.1	19.4	13.3	±5.11	1.12
NEE (μmol m <sup>−2</sup> s <sup>−1</sup> )	−1.14	±1.8	4.1	−2.4	±2.9	6.7
RECO (μmol m <sup>−2</sup> s <sup>−1</sup> )	10.13	±3.4	18.8	8.5	±3.0	15.2



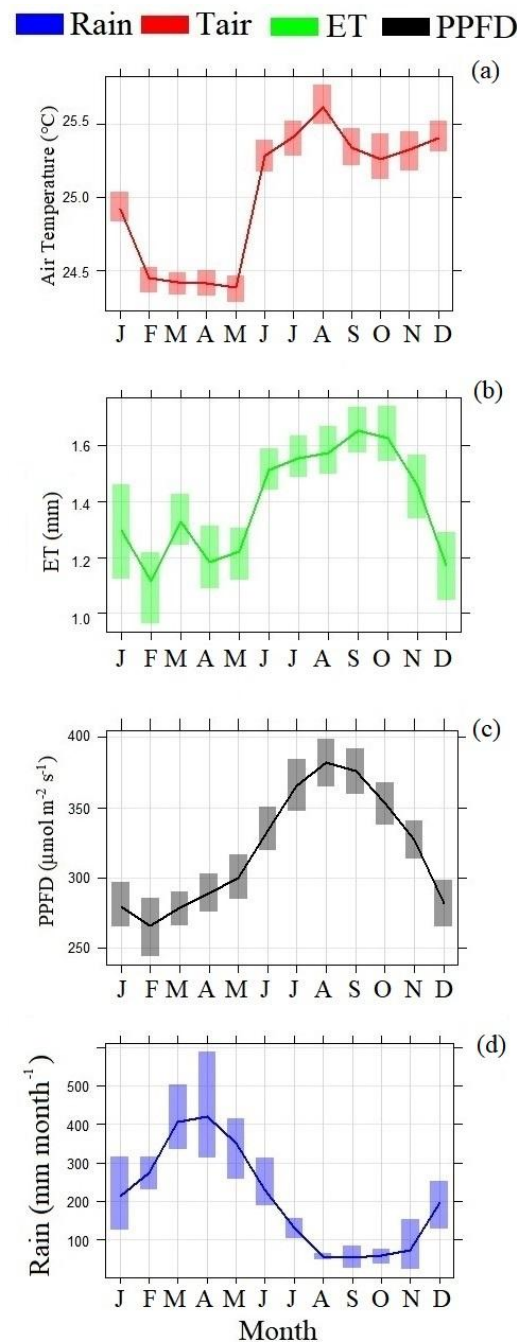


**Figure 4.** Monthly averages of (a) air temperature ( $^{\circ}\text{C}$ ), (b) Evapotranspiration (mm), (c) photosynthetic photon flux density ( $\mu\text{mol m}^{-2} \text{s}^{-1}$ ) and (d) precipitation ( $\text{mm month}^{-1}$ ) at Caxiuanã-PA site. The hatched area indicates the 95% confidence interval.

The three main components of the ecosystem's energy flux are shown in Figure 5. Net radiation ( $R_n$ ) was the main energy input to the ecosystem studied and drove other processes, such as evapotranspiration, the ecosystem's gross productivity, and temperature changes. The average daily  $R_n$  peak showed seasonal variations with higher values in the dry season (above  $300 \text{ W m}^{-2}$ ) than in the rainy season. Sensible heat flow ( $H$ ) did not show such an intense pattern (below  $100 \text{ W m}^{-2}$ ) compared to latent heat flow ( $LE$ ), which dominates the partitioning of available energy throughout the year and showed daily averages of up to  $200 \text{ W m}^{-2}$  at the height of the dry season.

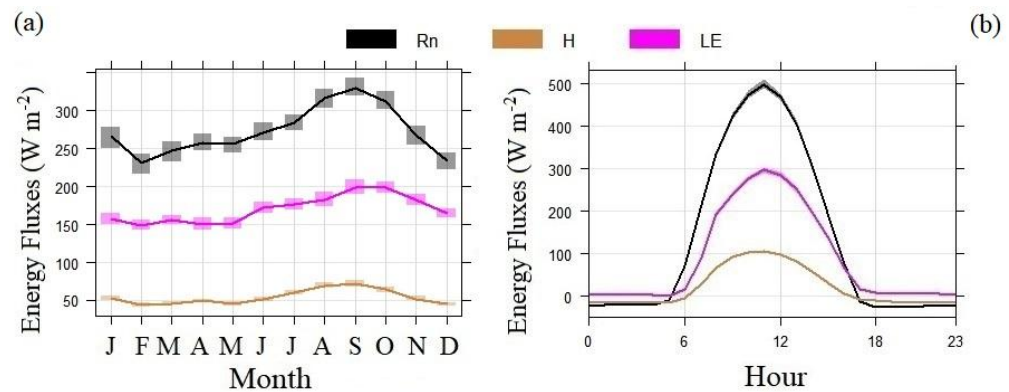


**Figure 5.** Monthly (a) and hourly (b) averages of the energy balance fluxes: radiation balance (Rn), sensible heat flux (H) and latent heat flux (LE), all in  $\text{W m}^{-2}$ . The hatched area indicates the 95% confidence interval.

### 3.2. Light Dependence Curves, Carbon Exchange and Vegetation Indices

Equation (6) describes the diurnal NEE in response to PAR, and this relationship for the Caxiuanã site is shown in Figure 6. It can be seen that the net  $\text{CO}_2$  absorption balance concomitantly increases with PAR. In addition, the  $\text{CO}_2$  flux decreases linearly with low solar radiation ( $\text{PAR} < 500 \mu\text{mol m}^{-2} \text{s}^{-1}$ ) in both the dry season (Figure 6a) and the rainy season (Figure 6b). The light saturation point varies according to the time of day, but it is generally above  $1000 \mu\text{mol m}^{-2} \text{s}^{-1}$ . The assimilation rate is higher in the afternoon for PAR values, which are up to  $1000 \mu\text{mol m}^{-2} \text{s}^{-1}$  in the dry season and up to around  $700 \mu\text{mol m}^{-2} \text{s}^{-1}$  in the rainy season.

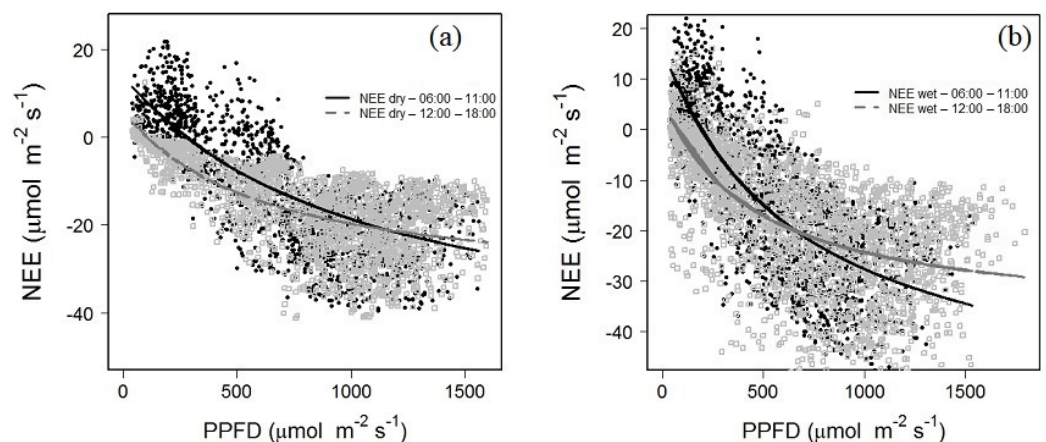


**Figure 6.** NEE response to PPFD in different seasons ((a) = dry; (b) = wet) and day periods.

There were no significant differences in the  $\text{CO}_2$  exchanges detected between the dry and rainy seasons (Figure 7). Both seasons showed a peak  $\text{CO}_2$  flux of around  $-20 \mu\text{mol CO}_2 \text{ m}^{-2} \text{s}^{-1}$ . The maximum gross productivity of the site occurred in February (Figure 8a), coinciding with the maximum absorption (most negative NEE) and minimum respiration of the ecosystem. The site behaves like a  $\text{CO}_2$  sink (negative NEE) for much of the year (from January to May and from September to December). On the other hand, during the dry season (from June to August) the site remained neutral. The seasonal dynamics of vegetation indices (EVI and NDVI) illustrate the pattern of land surface phenology in terms of vegetative canopy structure and vegetation cover development (Figure 8b), which clearly shows that vegetation seasonality is highly responsive to the environmental conditions of the location (Figure 2).

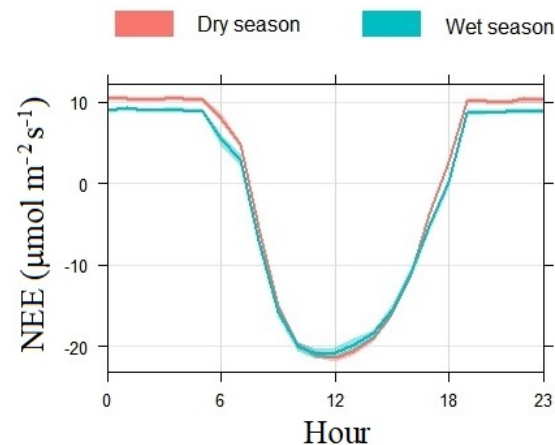


**Figure 7.** Average diurnal cycle of NEE at Caxiuanã, representing the CO<sub>2</sub> flux above the canopy, for the dry and rainy seasons. The hatched area indicates the 95% confidence interval.

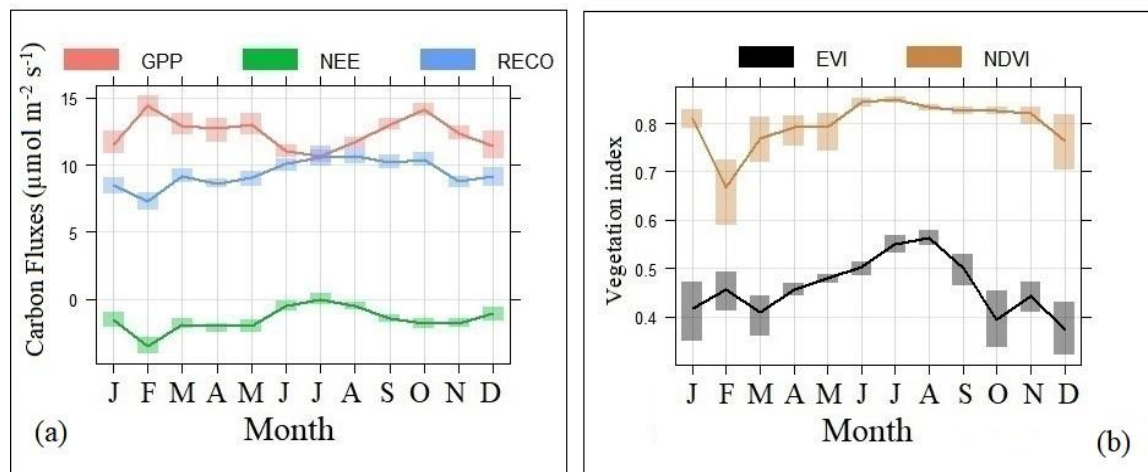
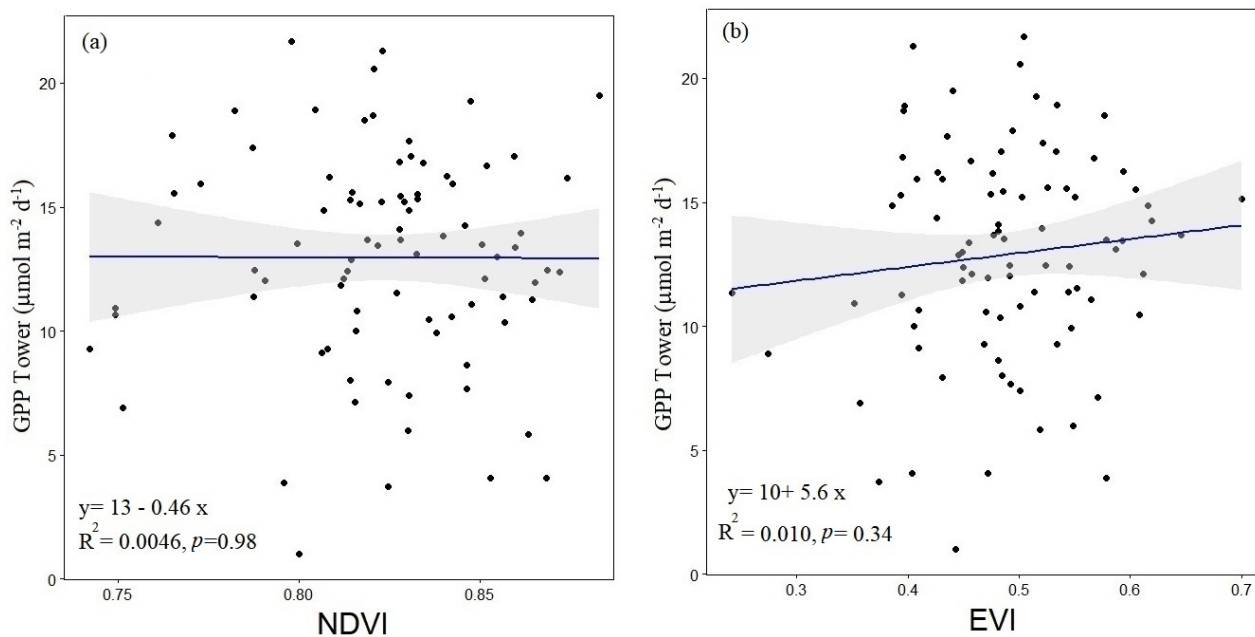


**Figure 8.** Monthly variation of NEE, GPP and RECO fluxes (a) and vegetation indices (b) at Caxiuanã. The hatched area indicates the 95% confidence interval.

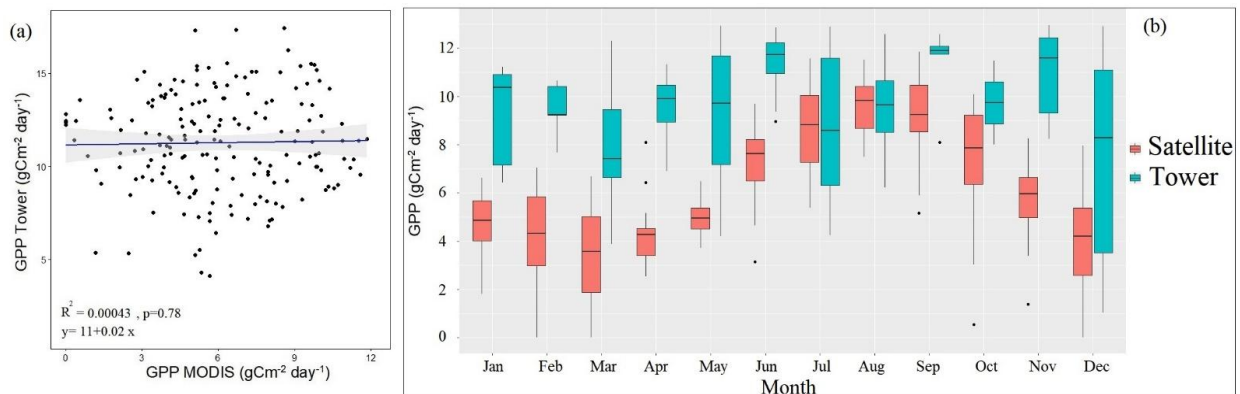
At the site under study, NDVI and EVI are highest in August (NDVI > 0.8; EVI > 0.5), following the course of the site's greater radiative supply, decreasing in intensity with decreases in solar radiation and air temperature, showing levels of NDVI < 0.8 and EVI < 0.5, indicating the onset of senescence. The linear correlations between NDVI and EVI with measured GPP (Figure 9) are irrelevant because they showed values close to 0.

Figure 9 shows the correlation between the GPP measured at the micrometeorological tower and the vegetation indices (NDVI and EVI) during the study years, with an insignificant correlation between GPP and EVI ( $R^2 = 0.01$ ) as well as with NDVI ( $R^2 = 0.0046$ ). As for the tower GPP X MODIS GPP data (Figure 10), the correlation between the data is insignificant (Figure 10a), and the greatest similarity between the measurements occurs in the months of July and August (Figure 10b), both due to the proximity of the medians and the magnitude of the monthly variability.

In the other months, there is a greater underestimation of MODIS GPP and a seasonal signal that does not accompany the measured data. The best association of the data occurs in the months with the highest LAI (Figure 11), which shows values of order  $> 6.0 \text{ m}^{-2} \text{ m}^{-2}$  and which are also the months with the lowest variability of the index, which shows a seasonal pattern that is highly related to the radiative availability of the site.



**Figure 9.** Pearson's linear correlation between the GPP data measured in the tower and the vegetation indices: NDVI (a) and EVI (b). The hatched area indicates the 95% confidence interval.



**Figure 10.** Comparison between measured gross primary production (Tower) and MODIS gross primary production (MODIS) in (a,b) Monthly GPP boxplot ( $\text{gC m}^{-2} \text{day}^{-1}$ ) for eddy covariance observed data (Tower) and MODIS—derived data (Satellite). The points refer to the outliers of the data, while the central lines refer to the median of each month.

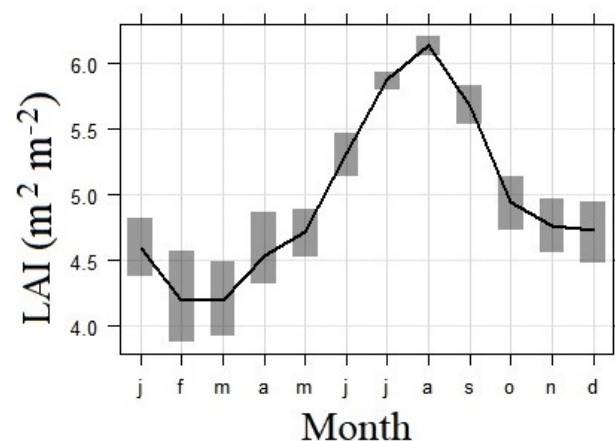


**Figure 11.** Monthly variation of LAI in the Caxiuanã site. The hatched area indicates the 95% confidence interval.



The carbon balance on the site (Figure 12a) is associated with local water availability (Figure 12b), where the greatest absorption (most negative NEE) occurred in 2006 ( $-979 \text{ g C m}^{-2} \text{ year}^{-1}$ ), which is later than the wettest year on the site (2005), which had an accumulated annual rainfall of  $2880 \text{ mm year}^{-1}$ . The year with the lowest absorption (least negative NEE) was 2008 ( $-27.6 \text{ g C m}^{-2} \text{ year}^{-1}$ ), which is after the year with the lowest annual rainfall ( $2105 \text{ mm year}^{-1}$ ) in 2007, indicating that the site's water availability can control the annual carbon balance in subsequent years.

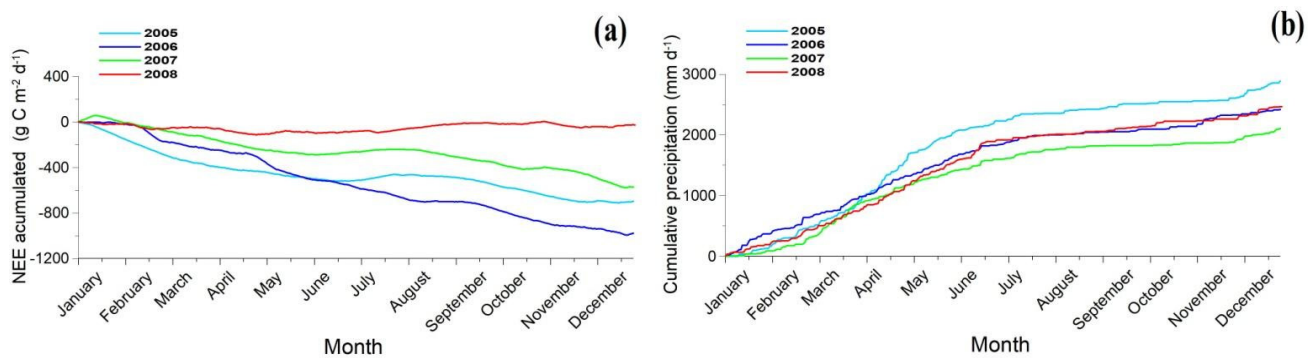


**Figure 12.** Annual carbon balance (a) and accumulated annual precipitation (b) at the Caxiuanã site for the years 2005 (aquamarine line), 2006 (blue line), 2007 (green line) and 2008 (red line).

#### 4. Discussion

The meteorological patterns corroborate those in the same study region for other periods [16,49,55] and show the particularity of the site compared to others in the Amazon, such as in the region of Santarém-PA, which has greater distributions of air temperature density above  $25^\circ \text{C}$  throughout the year [21] and has greater rainfall variability in the month of December. Seasonal changes in cloud cover are the main factors that determine the variation in solar radiation, even greater than the solar angle [69], which explains the increase in PPFD to the same extent as the decrease in precipitation.

Analyzing ET and precipitation, there is an increase in ET even in the less rainy period, which can be explained by the fact that primary forest is still a very humid environment and by the local floristic composition, with trees with deep root systems that seek water in the deeper layers of the soil, thus continuing the physiological activity of transpiration and maintaining the flow of water in the biosphere–atmosphere system. The seasonal variability that occurs in energy flows during the rainy and dry periods is noticeable, and this variability is explained by the high incidence of cloudiness that occurs in the Amazon basin, which is partly responsible for the increase in diffuse radiation and the decreases in radiation balance values [70], while during the dry period, it is characterized by less cloud presence, which results in an increase in the amount of net energy available to carry out the different processes that occur at the surface–atmosphere interface, reaching its maximum. The pattern of energy fluxes accompanying energy supply corroborates other studies [16,19,57] for this type of forest, unlike other areas where energy supply does not correspond to increases in other flows, such as LE, due to plant stomatal control mechanisms that cause the lowest ET values to occur at the end of the dry season [71]. For the Amazon rainforest, [72] also found distinct patterns of light dependence for the period before and after 11:30 a.m., but for other types of forest, even in the Amazon, the greatest assimilation occurs strictly in the daytime period [17].

Martínez et al. [73] showed that the coefficients of determination between NDVI and GPP are extremely low ( $R^2 < 0.2$ ) for grasslands and evergreen broad-leaved forests, a pattern similar to the Caxiuanã forest. For many forest sites, NDVI is more sensitive to vegetation change because its mathematical formulation is based on the ratio of the difference in infrared and the sum of red reflectance and the sum of red and infrared reflectance, which is not the case in this environment even with EVI, which is an enhancement of NDVI

because its mathematical formulation uses not only infrared and red reflectance but also surface cover and ground effects [61].

Zhang et al. [74] evaluated the spatial and temporal patterns of MODIS GPP at 40 sites located in the United States, comparing them with results from an ecosystem process model and with measurements of turbulent vortices (eddy covariance). It was found that there was an underestimation of MODIS GPP in highly productive months and an overestimation in low productivity months. This type of analysis is hampered in the study region and in almost the entire Amazon by the location's frequent cloud cover, which directly affects the images from optical sensors [75]. Although satellite remote sensing provides a viable and comprehensive means of observing environmental and phenological variations in the Amazon in a spatially wide-ranging and temporally frequent basis, the optical assessment of tropical areas is compromised by the high concentration of aerosols (biomass burning) and clouds [76–78], requiring the development of techniques for detecting clouds in images and improving estimates.

The authors suggest that the failure of the MODIS algorithm to represent the monthly and annual variability of GPP may be associated with the inadequacy of light use efficiency (LUE) models in capturing changes in canopy physiology over time. The tendencies in the MODIS GPP in relation to the observed data stem from a lack of sensitivity to canopy density, which is spatially and temporally variable. Other studies [79] evaluated the performance of GPP-MODIS in areas of the Brazilian Amazon, and they found that the MOD17 GPP product presented limitations in estimating the seasonality, magnitude and spatial variations of GPP in the tropical sites studied. When comparing MODIS GPP products with tower data in the Amazon, Nagai et al. [80] argue that the relationship between tower and image data is influenced by the satellite observation conditions and differences in scale, and despite this, it is possible to observe indices such as NDVI and EVI following the pattern of GPP increases from the beginning to the end of the dry season, suggesting changes in the structure and amount of water in the canopy seen by the sensor during the period of water stress and greater availability of radiation.

MOD17 overestimated GPP in low-productivity sites and underestimated it in high-productivity sites. Such results were also obtained in the literature [81,82]. The average annual carbon balance,  $-569.7 \pm 444.9 \text{ g C m}^{-2} \text{ year}^{-1}$ , is similar in magnitude to other tropical forest sites with high annual assimilation, as pointed out for the same site [17] in this study in a different period ( $-560 \text{ g C m}^{-2} \text{ year}^{-1}$ ), sites like the Cuieiras [34] reserve ( $-590 \text{ g C m}^{-2} \text{ year}^{-1}$ ) and a site [83] in Rondônia ( $-400 \text{ g C m}^{-2} \text{ year}^{-1}$ ). There are studies that show strong correlations between MODIS data and flux tower data ( $R^2 = 0.70$  in Temperate grassland, Zhu et al. [84]), while there are also sites where there is no or very weak correlation ( $R^2 = 0.01$  in Floodplain forest, Costa et al. [7];  $R^2 = 0.16$  in tropical peatland, Wang et al., [85];  $R^2 = 0.17$  in Alpine Grassland, Zhu et al. [84]).

These differences between satellite and tower data correlation need to be further studied for each type of environment, then it will be possible to identify places where we have poor estimates so the scientific community can propose other tools and methods to improve these estimates to compensate for the lack of information for remote areas with low densities of measured data, such as the site under study. Viable options for solving this problem today range from changing the parameters used to calculate satellite GPP, which is often stationary throughout the year, to applying machine learning techniques to improve estimates.

Although other sites in Amazonia have been shown to be moderate sources of  $\text{CO}_2$  to the atmosphere [36,57], the Caxiuanã site has been shown to be a considerable sink, with circulation patterns consistent with the literature [86], although it appears that precipitation can bring it to a state of neutrality in drier years. It is important to emphasize that there are many uncertainties associated with nocturnal respiration with gap filling by  $u^*$  at times of weak flows, which is true for practically all studies using the eddy covariance technique.

It is well known that the choice of  $u^*$  threshold for gap-filling corrections can lead to indirect measurements due to data substitution during periods of weak turbulence, and they

can even change the final results of a site from source to sink or sink to source [87]. However, gap-filling is accepted by the scientific community as necessary, and the automation of these gaps with valid data under similar environmental conditions as the filled data [88] provide confidence that the uncertainty of the data does not exceed acceptable percentage limits for a gap-fill, hence its widespread use by the scientific community [89].

## 5. Conclusions

The data show a forest area with well-defined seasonal patterns, with energy and water flows being controlled by radiative availability, and CO<sub>2</sub> seasonality patterns being controlled by the water available the previous year, probably due to the speed of the forest's physiological responses to environmental changes in a given year. In a climate-change context with an increase in the frequency of extreme weather events, this information is important to inform public policies on environmental conservation that can be adopted by the Brazilian government to mitigate these effects on this type of environment. We conclude that the site behaves as a CO<sub>2</sub> sink, like other parts of the Amazon rainforest reported in the literature, with latent heat flux dominating energy partitioning throughout the year and marked seasonality in meteorological variables. The satellite estimates show low correlation with the in situ data, as found in other similar sites in the literature, indicating the need for adjustments to the satellite parameters to better capture the seasonality of carbon exchange at the site. NDVI and EVI patterns follow radiative availability, as does LAI, but without direct capture related to GPP data, which correlates better with satellite data only in the months with the highest LAI. Carbon accumulations are shown to be directly related to the previous year's rainfall at the site, with the intensity of capture varying according to the increase or decrease in precipitation accumulations. In a global context where there is a great call to value the standing forest due to its ecosystem services and the great profits that the bioeconomy can provide to the communities that depend on the forest, the results of this work serve as a basis for showing the importance of conserving the environment studied here as a tool for mitigating climate change.

**Author Contributions:** Conceptualization, M.P.A., R.A.S. and G.B.-C.; Methodology, C.M.S.e.S., B.G.B., K.R.M., M.L.B., R.A.S., L.V.P., A.S.d.S., W.B.M., I.M.S.R., M.C.d.R.S. and G.B.-C.; Software, M.L.B., H.G.G.C.N., W.B.M., M.C.d.R.S., A.B.d.S.G. and G.B.-C.; Validation, C.M.S.e.S., K.R.M., J.G.M.D.S., T.T.d.A.T.N., I.M.S.R., M.C.d.R.S., A.B.d.S.G. and G.B.-C.; Formal analysis, M.P.A., C.M.S.e.S., K.R.M., H.G.G.C.N., T.T.d.A.T.N., A.S.d.S., V.H.P.M., I.M.S.R. and W.P.; Investigation, M.P.A., B.G.B., K.R.M., J.G.M.D.S., T.T.d.A.T.N., A.S.d.S., W.P. and G.B.-C.; Resources, R.B.C.d.S.; Data curation, L.V.P.; Writing—original draft, L.A.M., H.G.G.C.N., L.V.P. and P.O.; Writing—review & editing, C.M.S.e.S., B.G.B., L.A.M. and P.O.; Visualization, J.G.M.D.S. and V.H.P.M.; Supervision, G.B.-C.; Project administration, R.B.C.d.S. All authors have read and agreed to the published version of the manuscript.

**Funding:** The authors are also thankful to the National Council for Scientific and Technological Development (CNPq) for the research productivity grant of C.M.S.e.S. (Process n° 303802/2017-0), the undergraduate research project (PIBIC—CNPq—UFOPA for M.L.B.), the grant of Productivity and Technological Development Scholarship Program (PQDT-UFOPA) to G.B.-C., the financial support of PROPESP/UFGA (PAPQ) and Research Incentive Program—PIP (PPBIO-UFOPA).

**Data Availability Statement:** The original contributions presented in the study are included in the article, further inquiries can be directed to the corresponding author.

**Conflicts of Interest:** The authors declare no conflicts of interest, and the funders had no role in the design of the study.

## References

1. Mendes, K.R.; Campos, S.; da Silva, L.L.; Mutti, P.R.; Ferreira, R.R.; Medeiros, S.S.; Perez-Marin, A.M.; Marques, T.V.; Ramos, T.M.; Vieira, M.M.d.L.; et al. Seasonal variation in net ecosystem CO<sub>2</sub> exchange of a Brazilian seasonally dry tropical forest. *Sci. Rep.* **2020**, *10*, 9454. [[CrossRef](#)]

2. Campos, S.; Mendes, K.R.; da Silva, L.L.; Mutti, P.R.; Medeiros, S.S.; Amorim, L.B.; dos Santos, C.A.; Perez-Marin, A.M.; Ramos, T.M.; Marques, T.V.; et al. Closure and partitioning of the energy balance in a preserved area of a Brazilian seasonally dry tropical forest. *Agric. For. Meteorol.* **2019**, *271*, 398–412. [\[CrossRef\]](#)
3. Marques, T.V.; Mendes, K.; Mutti, P.; Medeiros, S.; Silva, L.; Perez-Marin, A.M.; Campos, S.; Lúcio, P.S.; Lima, K.; dos Reis, J.; et al. Environmental and biophysical controls of evapotranspiration from Seasonally Dry Tropical Forests (Caatinga) in the Brazilian Semiarid. *Agric. For. Meteorol.* **2020**, *287*, 107957. [\[CrossRef\]](#)
4. Silva, A.C.; Mendes, K.R.; e Silva, C.M.S.; Rodrigues, D.T.; Costa, G.B.; da Silva, D.T.C.; Mutti, P.R.; Ferreira, R.R.; Bezerra, B.G. Energy Balance, CO<sub>2</sub> Balance, and Meteorological Aspects of Desertification Hotspots in Northeast Brazil. *Water* **2021**, *13*, 2962. [\[CrossRef\]](#)
5. Silva, C.M.S.; Bezerra, B.G.; Mendes, K.R.; Mutti, P.R.; Rodrigues, D.T.; Costa, G.B.; de Oliveira, P.E.S.; Reis, J.; Marques, T.V.; Ferreira, R.R.; et al. Rainfall and rain pulse role on energy, water vapor and CO<sub>2</sub> exchanges in a tropical semiarid environment. *Agric. For. Meteorol.* **2024**, *345*, 109829. [\[CrossRef\]](#)
6. Mendes, K.R.; Marques, A.M.S.; Mutti, P.R.; Oliveira, P.E.S.; Rodrigues, D.T.; Costa, G.B.; Ferreira, R.R.; Silva, A.C.N.d.; Morais, L.F.; Lima, J.R.S.; et al. Interannual Variability of Energy and CO<sub>2</sub> Exchanges in a Remnant Area of the Caatinga Biome under Extreme Rainfall Conditions. *Sustainability* **2023**, *15*, 10085. [\[CrossRef\]](#)
7. Costa, G.B.; Mendes, K.R.; Viana, L.B.; Almeida, G.V.; Mutti, P.R.; Silva, C.M.S.e.; Bezerra, B.G.; Marques, T.V.; Ferreira, R.R.; Oliveira, C.P.; et al. Seasonal Ecosystem Productivity in a Seasonally Dry Tropical Forest (Caatinga) Using Flux Tower Measurements and Remote Sensing Data. *Remote Sens.* **2022**, *14*, 3955. [\[CrossRef\]](#)
8. Bezerra, B.G.; e Silva, C.M.S.; Mendes, K.R.; Mutti, P.R.; Fernandes, L.S.; Marques, T.V.; Silva, C.L.C.; Campos, S.; de Lima Vieira, M.M.; Urbano, S.A.; et al. CO<sub>2</sub> exchanges and evapotranspiration of a grazed pasture under tropical climate conditions. *Agric. For. Meteorol.* **2022**, *323*, 109088. [\[CrossRef\]](#)
9. Da Silva, I.W.H.; Marques, T.V.; Urbano, S.A.; Mendes, K.R.; Oliveira, A.C.C.F.; Nascimento, F.D.S.; De Morais, L.F.; Pereira, W.; Dos, S.; Mutti, P.R.; et al. Meteorological and biophysical controls of evapotranspiration in tropical grazed pasture under rainfed conditions. *Agric. Water Manag.* **2024**, *299*, 108884. [\[CrossRef\]](#)
10. Vourlitis, G.L.; Filho, N.P.; Hayashi, M.M.S.; Nogueira, J.d.S.; Caseiro, F.T.; Campelo, J.H. Seasonal variations in the evapotranspiration of a transitional tropical forest of Mato Grosso, Brazil. *Water Resour. Res.* **2002**, *38*, 1094. [\[CrossRef\]](#)
11. Silva, J.B.; Valle Junior, L.C.G.; Faria, T.O.; Marques, J.B.; Dalmagro, H.J.; Nogueira, J.S.; Vourlitis, G.L.; Rodrigues, T.R. Temporal Variability in Evapotranspiration and Energy Partitioning over a Seasonally Flooded Scrub Forest of the Brazilian Pantanal. *Agric. For. Meteorol.* **2021**, *308*, 108559. [\[CrossRef\]](#)
12. Rocha, H.R.; Freitas, H.C.; Rosolem, R.; Juárez, R.I.; Tannus, R.N.; Ligo, M.A.; Cabral, O.M.R.; Dias, M.A.S. Measurements of CO<sub>2</sub> exchange over a woodland savanna (Cerrado Ssensu stricto) in southeast Brasil. *Biota Neotrop.* **2002**, *2*, 1–11. [\[CrossRef\]](#)
13. von Randow, C.; Zeri, M.; Restrepo-Coupe, N.; Muza, M.N.; de Gonçalves, L.G.G.; Costa, M.H.; Araujo, A.C.; Manzi, A.O.; da Rocha, H.R.; Saleska, S.R.; et al. Inter-annual variability of carbon and water fluxes in Amazonian forest, Cerrado and pasture sites, as simulated by terrestrial biosphere models. *Agric. For. Meteorol.* **2013**, *182*, 145–155. [\[CrossRef\]](#)
14. Araújo, A.C.; Nobre, A.D.; Kruijt, B.; Elbers, J.A.; Dallarosa, R.; Stefani, P.; Randow, C.; von Manzi, A.O.; Culf, A.D.; Gash, J.H.C.; et al. Comparative measurements of carbon dioxide fluxes from two nearby towers in a central Amazonian rainforest: The Manaus LBA site. *J. Geophys. Res.* **2002**, *107*, 8090. [\[CrossRef\]](#)
15. dos Santos, A.F.; Moura, F.R.T.; Seruffo, M.C.d.R.; dos Santos, W.P.; Costa, G.B.; Costa, F.A.R. The impact of meteorological changes on the quality of life regarding thermal comfort in the Amazon region. *Front. Clim.* **2023**, *5*, 1126042. [\[CrossRef\]](#)
16. Carswell, F.E.; Costa, A.L.; Palheta, M.; Malhi, Y.; Meir, P.; Costa, J.D.P.; Ruivo, M.D.L.; Leal, L.D.S.; Costa, J.M.N.; Clement, R.J.; et al. Seasonality in CO<sub>2</sub> and H<sub>2</sub>O flux at an eastern Amazonian rain forest. *J. Geophys. Res.* **2002**, *107*, 16. [\[CrossRef\]](#)
17. Hutyrá, L.R.; Munger, J.W.; Hammond-Pyle, E.; Saleska, S.R.; Restrepo-Coupe, N.; Daube, B.C.; de Camargo, P.B.; Wofsy, S.C. Resolving systematic errors in estimates of net ecosystem exchange of CO<sub>2</sub> and ecosystem respiration in a tropical forest biome. *Agric. For. Meteorol.* **2008**, *148*, 1266–1279. [\[CrossRef\]](#)
18. Costa, G.; Da Rocha, H.R.; De Freitas, H.C. Fluxo De CH<sub>4</sub> em Área de Floresta Às Margens Do Rio Araguaia-MT. *Ciência Nat.* **2016**, *38*, 163. [\[CrossRef\]](#)
19. Rocha, H.R.; Manzi, A.O.; Cabral, O.M.; Miller, S.D.; Goulden, M.L.; Saleska, S.R.; R-Coupe, N.; Wofsy, S.C.; Borma, L.S.; Artaxo, P.; et al. Patterns of water and heat flux across a biome gradient from tropical forest to savanna in Brazil. *J. Geophys. Res.* **2009**, *114*, 8. [\[CrossRef\]](#)
20. Costa, G.B.; Santos e Silva, C.M.; Mendes, K.R.; dos Santos, J.G.M.; Neves, T.T.A.T.; Silva, A.S.; Rodrigues, T.R.; Silva, J.B.; Dalmagro, H.J.; Mutti, P.R.; et al. WUE and CO<sub>2</sub> Estimations by Eddy Covariance and Remote Sensing in Different Tropical Biomes. *Remote Sens.* **2022**, *14*, 3241. [\[CrossRef\]](#)
21. Costa, G.; Silva, C.; Mendes, K.R.; Bezerra, B.; Rodrigues, T.R.; Silva, J.B.; Dalmagro, H.J.; Nunes, H.; Gomes, A.; Silva, G.; et al. The Relevance of Maintaining Standing Forests for Global Climate Balance: A Case Study in Brazilian Forests. In *Tropical Forests—Ecology, Diversity and Conservation Status*, 1st ed.; Carmona, E.C., Musarella, C.M., Ortiz, A.C., Eds.; InTech Open: London, UK, 2023; Volume 1, pp. 1–17. [\[CrossRef\]](#)
22. Mendes, K.R.; Batista-Silva, W.; Dias-Pereira, J.; Pereira, M.P.S.; Souza, E.V.; Serrão, J.E.; Granja, J.A.A.; Pereira, E.C.; Gallacher, D.J.; Mutti, P.R.; et al. Leaf plasticity across wet and dry seasons in *Croton blanchetianus* (Euphorbiaceae) at a tropical dry forest. *Sci. Rep.* **2022**, *12*, 954. [\[CrossRef\]](#)



23. Zhang, T.; Song, B.; Han, G.; Zhao, H.; Hu, Q.; Zhao, Y.; Liu, H. Effects of coastal wetland reclamation on soil organic carbon, total nitrogen, and total phosphorus in China: A meta-analysis. *Land Degrad. Dev.* **2023**, *34*, 3340–3349. [\[CrossRef\]](#)
24. Zhao, Y.; Yi, J.; Yao, R.; Li, F.; Hill, R.L.; Gerke, H.H. Dimensionality and scales of preferential flow in soils of Shale Hills hillslope simulated using HYDRUS. *Vadose Zone J.* **2024**, *23*, e20367. [\[CrossRef\]](#)
25. Zhou, G.; Liu, W.; Zhu, Q.; Lu, Y.; Liu, Y. ECA-MobileNetV3(Large)+SegNet Model for Binary Sugarcane Classification of Remotely Sensed Images. *IEEE Trans. Geosci. Remote Sens.* **2022**, *60*, 4414915. [\[CrossRef\]](#)
26. Covey, K.; Soper, F.; Pangala, S.; Bernardino, A.; Pagliaro, Z.; Basso, L.; Cassol, H.; Fearnside, P.; Navarrete, D.; Novoa, S.; et al. Carbon and beyond: The biogeochemistry of climate in a rapidly changing Amazon. *Front. For. Glob. Chang.* **2021**, *4*, 11. [\[CrossRef\]](#)
27. Nobre, C.A.; Sampaio, G.; Borma, L.S.; Castilla-Rubio, J.C.; Silva, J.S.; Cardoso, M. Land-use and climate change risks in the Amazon and the need of a novel sustainable development paradigm. *Proc. Natl. Acad. Sci. USA* **2016**, *113*, 10759–10768. [\[CrossRef\]](#)
28. Qiu, S.; Yang, H.; Zhang, S.; Huang, S.; Zhao, S.; Xu, X.; He, P.; Zhou, W.; Zhao, Y.; Yan, N.; et al. Carbon storage in an arable soil combining field measurements, aggregate turnover modeling and climate scenarios. *Catena* **2023**, *220*, 106708. [\[CrossRef\]](#)
29. Zhou, G.; Xu, C.; Zhang, H.; Zhou, X.; Zhao, D.; Wu, G.; Lin, J.; Liu, Z.; Yang, J.; Nong, X.; et al. PMT gain self-adjustment system for high-accuracy echo signal detection. *Int. J. Remote Sens.* **2022**, *43*, 7213–7235. [\[CrossRef\]](#)
30. Wang, Y.; Quan, S.; Tang, X.; Hosono, T.; Hao, Y.; Tian, J.; Pang, Z. Organic and Inorganic Carbon Sinks Reduce Long-Term Deep Carbon Emissions in the Continental Collision Margin of the Southern Tibetan Plateau: Implications for Cenozoic Climate Cooling. *J. Geophys. Res. Solid Earth* **2024**, *129*, e2024JB028802. [\[CrossRef\]](#)
31. Wofsy, S.C.; Harriss, R.C.; Kaplan, W.A. Carbon dioxide in the atmosphere over the Amazon Basin. *J. Geophys. Res. Earth Surf.* **1988**, *93*, 1377–1387. [\[CrossRef\]](#)
32. Phillips, O.L.; Brienen, R.J.W.; Gloor, E.; Baker, T.R.; Lloyd, J.; Lopez-Gonzalez, G.; Monteagudo-Mendoza, A.; Malhi, Y.; Lewis, S.L.; Vásquez Martínez, R.; et al. Carbon Uptake by Mature Amazon Forests Has Mitigated Amazon Nations' Carbon Emissions. *Carbon Balance Manag.* **2017**, *12*, 1–9. [\[CrossRef\]](#)
33. Grace, J.; Lloyd, J.; McIntyre, J.; Miranda, A.C.; Meir, P.; Miranda, H.; Moncrieff, J.M.; Massheder, J.; Wright, I.R.; Gash, J. Fluxes of carbon dioxide and water vapour over an undisturbed tropical rainforest in south-west Amazonia. *Glob. Chang. Biol.* **1995**, *1*, 1–12. [\[CrossRef\]](#)
34. Malhi, Y.; Nobre, A.; Grace, J.; Kruijt, B.; Pereira, M.; Culf, A.; Scott, S. Carbon dioxide transfer over a Central Amazonian rain forest. *J. Geophys. Res.* **1998**, *103*, 31593–31612. [\[CrossRef\]](#)
35. Keller, M.; Alencar, A.; Asner, G.P.; Braswell, B.; Bustamante, M.; Davidson, E.; Feldpausch, T.; Fernandes, E.; Goulden, M.; Kabat, P.; et al. Ecological research in the large-scale biosphere–atmosphere experiment in Amazonia: Early results. *Ecol. Appl.* **2004**, *14*, S3–S16. [\[CrossRef\]](#)
36. Saleska, S.R.; Millar, S.D.; Martos, D.M.; Goulden, M.L.; Wofsy, S.C.; da Rocha, H.R.; de Camargo, P.B.; Crill, P.; Daule, B.C.; de Freitas, H.C.; et al. Carbon in Amazon forests, unexpected seasonal fluxes and disturbance-induced losses. *Science* **2003**, *302*, 1554–1557. [\[CrossRef\]](#)
37. Miller, S.D.; Goulden, M.L.; Menton, M.C.; Da Rocha, H.R.; De Freitas, H.C.; Figueira, A.M.S.; Sousa, C.A.D. Biometric and micrometeorological measurements of tropical forest carbon balance. *Ecol. Appl.* **2004**, *14*, S114–S126. [\[CrossRef\]](#)
38. Espírito-Santo, F.D.; Gloor, M.; Keller, M.; Malhi, Y.; Saatchi, S.; Nelson, B.; Junior, R.C.O.; Pereira, C.; Lloyd, J.; Froliking, S.; et al. Size and frequency of natural forest disturbances and the Amazon forest carbon balance. *Nat. Commun.* **2014**, *5*, 3434. [\[CrossRef\]](#)
39. Zhou, G.; Zhang, H.; Xu, C.; Zhou, X.; Liu, Z.; Zhao, D.; Lin, J.; Wu, G. A Real-Time Data Acquisition System for Single-Band Bathymetric LiDAR. *IEEE Trans. Geosci. Remote Sens.* **2023**, *61*, 5702721. [\[CrossRef\]](#)
40. Fan, X.; Hu, Z.; Zhao, Y.; Chen, J.; Wei, T.; Huang, Z. A Small-Ship Object Detection Method for Satellite Remote Sensing Data. *IEEE J. Sel. Top. Appl. Earth Obs. Remote Sens.* **2024**, *17*, 11886–11898. [\[CrossRef\]](#)
41. Sun, L.; Wang, X.; Zheng, Y.; Wu, Z.; Fu, L. Multiscale 3-D–2-D Mixed CNN and Lightweight Attention-Free Transformer for Hyperspectral and LiDAR Classification. *IEEE Trans. Geosci. Remote Sens.* **2024**, *62*, 2100116. [\[CrossRef\]](#)
42. Chen, X.; Xie, D.; Zhang, Z.; Sharma, R.P.; Chen, Q.; Liu, Q.; Fu, L. Compatible Biomass Model with Measurement Error Using Airborne LiDAR Data. *Remote Sens.* **2023**, *15*, 3546. [\[CrossRef\]](#)
43. Zhang, Z.; Xu, Y.; Song, J.; Zhou, Q.; Rasol, J.; Ma, L. Planet craters detection based on unsupervised domain adaptation. *IEEE Trans. Aerosp. Electron. Syst.* **2023**, *59*, 7140–7152. [\[CrossRef\]](#)
44. Yin, Z.; Liu, Z.; Liu, X.; Zheng, W.; Yin, L. Urban heat islands and their effects on thermal comfort in the US: New York and New Jersey. *Ecol. Indic.* **2023**, *154*, 110765. [\[CrossRef\]](#)
45. Shang, K.; Xu, L.; Liu, X.; Yin, Z.; Liu, Z.; Li, X.; Yin, L.; Zheng, W. Study of Urban Heat Island Effect in Hangzhou Metropolitan Area Based on SW-TES Algorithm and Image Dichotomous Model. *SAGE Open* **2023**, *13*, 1–20. [\[CrossRef\]](#)
46. Chen, J.; Zhao, Z.; Yang, Y.; Li, C.; Yin, Y.; Zhao, X.; Zhao, N.; Tian, J.; Li, H. Metallogenic prediction based on fractal theory and machine learning in Duobaoshan Area, Heilongjiang Province. *Ore Geol. Rev.* **2024**, *168*, 106030. [\[CrossRef\]](#)
47. Myneni, R.B.; Yang, W.; Nemani, R.R.; Huete, A.R.; Dickinson, R.E.; Knyazikhin, Y.; Didan, K.; Fu, R.; Juárez, R.I.N.; Saatchi, S.S.; et al. Large seasonal swings in leaf area of Amazon rainforests. *Proc. Natl. Acad. Sci. USA* **2007**, *104*, 4820–4823. [\[CrossRef\]](#)
48. Huete, A.R.; Didan, K.; Shimabukuro, Y.E.; Ratana, P.; Saleska, S.R.; Hutya, L.R.; Yang, W.; Nemani, R.R.; Myneni, R. Amazon rainforests green-up with sunlight in dry season. *Geophys. Res. Lett.* **2006**, *33*, 1–4. [\[CrossRef\]](#)

49. Silva, R.M.D.; Costa, J.M.N.D.; Ruivo, M.D.L.P.; Costa, A.C.L.D.; Almeida, S.S. Influence of meteorological variables in the litterfall production in the Ferreira Penna Scientific Station, Caxiuanã, Pará, Brazil. *Acta Amaz.* **2009**, *39*, 573–582. [\[CrossRef\]](#)
50. Costa, A.C.L.; Metcalfe, D.B.; Doughty, C.E.; de Oliveira, A.A.R.; Neto, G.F.C.; da Costa, M.C.; Silva Junior, J.D.A.; Aragão, L.E.O.C.; Almeida, S.; Galbraith, D.R.; et al. Ecosystem respiration and net primary productivity after 8–10 years of experimental through-fall reduction in an eastern Amazon forest. *Plant Ecol. Divers.* **2014**, *7*, 7–24. [\[CrossRef\]](#)
51. Baldocchi, D.; Chu, H.; Reichstein, M. Inter-Annual Variability of Net and Gross Ecosystem Carbon Fluxes: A Review. *Agric. For. Meteorol.* **2018**, *249*, 520–533. [\[CrossRef\]](#)
52. Hu, Z.M.; Piao, S.L.; Knapp, A.K.; Wang, X.H.; Peng, S.S.; Yuan, W.P.; Running, S.; Mao, J.F.; Shi, X.Y.; Ciais, P.; et al. Decoupling of greenness and gross primary productivity as aridity decreases. *Remote Sens. Environ.* **2022**, *279*, 10. [\[CrossRef\]](#)
53. da Silva Ataíde, W.L.; de Oliveira, F.D.A.; Pinto, C.A.D. Balance of radiation, energy and balance closure in a pristine forest in the eastern Amazon. *Rev. Bras. Geogr. Física* **2020**, *13*, 2603–2627.
54. Kotteck, M.; Grieser, J.; Beck, C.; Rudolf, B.; Rubel, F. World-Map of the Köppen-Geiger climate classification updated. *Meteorol. Z.* **2006**, *15*, 259–263. [\[CrossRef\]](#) [\[PubMed\]](#)
55. da Costa, A.C.L.; Galbraith, D.; Almeida, S.; Portela, B.T.T.; da Costa, M.; de Athaydes Silva Junior, J.; Braga, A.P.; de Gonçalves, P.H.; de Oliveira, A.A.; Fisher, R.; et al. Effect of 7 yr of experimental drought on vegetation dynamics and biomass storage of an eastern Amazonian rainforest. *N. Phytol.* **2010**, *187*, 579–591. [\[CrossRef\]](#)
56. Souza Filho, J.D.C.; Ribeiro, A.; Cohen, J.C.P. Seasonal variation of radiation in a tropical forest in northeastern Amazonia. *Rev. Bras. Meteorol.* **2006**, *21*, 318–330.
57. Hutyra, L.R.; Munger, J.W.; Saleska, S.R.; Gottlieb, E.; Daube, B.C.; Dunn, A.L.; Amaral, D.F.; de Camargo, P.B.; Wofsy, S.C. Seasonal controls on the exchange of carbon and water in an Amazonian rain forest. *J. Geophys. Res.* **2007**, *112*, 1–16.
58. Baldocchi, D.D. Assessing the eddy covariance technique for evaluating carbon dioxide exchange rates of ecosystems: Past, present and future. *Glob. Chang. Biol.* **2003**, *9*, 479–492. [\[CrossRef\]](#)
59. Hilker, T.; Galvão, L.S.; Aragão, L.E.; de Moura, Y.M.; Amaral, C.H.D.; Lyapustin, A.I.; Wu, J.; Albert, L.P.; Ferreira, M.J.; Anderson, L.O.; et al. Vegetation chlorophyll estimates in the Amazon from multi-angle MODIS observations and canopy reflectance model. *Int. J. Appl. Earth Obs. Geoinf.* **2017**, *58*, 278–287. [\[CrossRef\]](#)
60. Myneni, R.; Knyazikhin, Y.; Park, T. MOD15A2H MODIS/Terra Leaf Area Index/FPAR 8-Day L4 Global 500m SIN Grid V006 [Data Set]. NASA EOSDIS Land Processes DAAC; NASA: Washington, DC, USA, 2015. [\[CrossRef\]](#)
61. Jiang, Z.; Huete, A.R.; Didan, K.; Miura, T. Development of a two-band enhanced vegetation index without a blue band. *Remote Sens. Environ.* **2008**, *112*, 3833–3845. [\[CrossRef\]](#)
62. Yang, W.; Tan, B.; Huang, D.; Rautiainen, M.; Shabanov, N.; Wang, Y.; Privette, J.; Huemmrich, K.; Fensholt, R.; Sandholt, I.; et al. MODIS leaf area index products: From validation to algorithm improvement. *IEEE Trans. Geosci. Remote Sens.* **2006**, *44*, 1885–1898. [\[CrossRef\]](#)
63. Monteith, J.L. Solar Radiation and Productivity in Tropical Ecosystems. *J. Appl. Ecol.* **1972**, *9*, 747. [\[CrossRef\]](#)
64. Boudriki Semlali, B.E.; El Amrani, C. Satellite Big Data Ingestion for Environmentally Sustainable Development. In *Emerging Trends in ICT for Sustainable Development: The Proceedings of NICE 2020 International Conference*; Springer International Publishing: Berlin/Heidelberg, Germany, 2021; pp. 269–284.
65. Boudriki Semlali, B.; El Amrani, C.; Ortiz, G.; Boubeta-Puig, J.; Garcia-De-Prado, A. SAT-CEP-monitor: An air quality monitoring software architecture combining complex event processing with satellite remote sensing. *Comput. Electr. Eng.* **2021**, *93*, 107257. [\[CrossRef\]](#)
66. Restrepo-Coupe, N.; da Rocha, H.R.; Hutyra, L.R.; da Araujo, A.C.; Borma, L.S.; Christoffersen, B.; Cabral, O.M.R.; de Camargo, P.B.; Cardoso, F.L.; da Costa, A.C.L.; et al. What drives the seasonality of photosynthesis across the Amazon basin? A cross-site analysis of eddy flux tower measurements from the Brasil flux network. *Agric. For. Meteorol.* **2013**, *819*, 128–144. [\[CrossRef\]](#)
67. Papale, D.; Reichstein, M.; Aubinet, M.; Canfora, E.; Bernhofer, C.; Kutsch, W.; Longdoz, B.; Rambal, S.; Valentini, R.; Vesala, T. Towards a standardized processing of Net Ecosystem Exchange measured with eddy covariance technique: Algorithms and uncertainty estimation. *Biogeosciences* **2006**, *3*, 571–583. [\[CrossRef\]](#)
68. Reichstein, M.; Falge, E.; Baldocchi, D.; Papale, D.; Aubinet, M.; Berbigier, P.; Bernhofer, C.; Buchmann, N.; Giulmanov, T.; Granier, A.; et al. On the separation of net ecosystem exchange into assimilation and ecosystem respiration: Review and improved algorithm. *Glob. Chang. Biol.* **2005**, *11*, 1424–1439. [\[CrossRef\]](#)
69. Malhi, Y.; Meir, P. An international network to understand the biomass and dynamics of Amazonian forests (RAINFOR). *J. Veg. Sci. Adv. Plant Community Ecol.* **2002**, *13*, 439–450.
70. Fitzjarrald, D.R.; Sakai, R.K.; Moraes, O.L.L.; De Oliveira, R.C.; Acevedo, O.C.; Czikowsky, M.J.; Beldini, T. Spatial and temporal rainfall variability near the amazon-tapajós confluence. *J. Geophys. Res. Biogeosci.* **2008**, *113*, G00B11. [\[CrossRef\]](#)
71. Fonseca, L.D.M.; Dalagnol, R.; Malhi, Y.; Rifai, S.W.; Costa, G.B.; Silva, T.S.F.; Da Rocha, H.R.; Tavares, I.B.; Borma, L.S. Phenology and Seasonal Ecosystem Productivity in an Amazonian Floodplain Forest. *Remote Sens.* **2019**, *11*, 1530. [\[CrossRef\]](#)
72. Goulden, M.L.; Miller, S.D.; Da Rocha, H.R.; Menton, M.C.; de Freitas, H.C.; e Silva Figueira, A.M.; de Sousa, C.A. Diel and seasonal patterns of tropical forest CO<sub>2</sub> exchange. *Ecol. Appl.* **2004**, *14*, 42–54. [\[CrossRef\]](#)
73. Fernández-Martínez, M.; Yu, R.; Gamon, J.; Hmimina, G.; Filella, I.; Balzarolo, M.; Stocker, B.; Peñuelas, J. Monitoring Spatial and Temporal Variabilities of Gross Primary Production Using MAIAC MODIS Data. *Remote Sens.* **2019**, *11*, 874. [\[CrossRef\]](#)

74. Zhang, Y.; Xiao, X.; Wu, X.; Zhou, S.; Zhang, G.; Qin, Y.; Dong, J. A global moderate resolution dataset of gross primary production of vegetation for 2000–2016. *Sci. Data* **2017**, *4*, 170165. [[CrossRef](#)] [[PubMed](#)]
75. Asner, G.P. Cloud cover in Landsat observations of the Brazilian Amazon. *Int. J. Remote Sens.* **2001**, *22*, 3855–3862. [[CrossRef](#)]
76. Artaxo, P.; Rizzo, L.V.; Brito, J.F.; Barbosa, H.M.J.; Arana, A.; Sena, E.T.; Cirino, G.G.; Bastos, W.; Martin, S.T.; Andreae, M.O. Atmospheric aerosols in Amazonia and land use change: From natural biogenic to biomass burning conditions. *Faraday Discuss.* **2013**, *165*, 203–235. [[CrossRef](#)] [[PubMed](#)]
77. Chen, T.C.; Yoon, J.H.; St Croix, K.J.; Takle, E.S. Suppressing impacts of the Amazonian deforestation by the global circulation change. *Bull. Amer. Met. Soc.* **2001**, *82*, 2209–2215. [[CrossRef](#)]
78. Hilker, T.; Lyapustin, A.I.; Tucker, C.J.; Hall, F.G.; Myneni, R.B.; Wang, Y.; Bi, J.; de Moura, Y.M.; Sellers, P.J. Vegetation dynamics and rainfall sensitivity of the Amazon. *Proc. Natl. Acad. Sci. USA* **2014**, *111*, 1604116046. [[CrossRef](#)]
79. Almeida, C.T.; Delgado, R.C.; Galvão, L.S.; de Oliveira Cruz e Aragão, L.E.; Ramos, M.C. Improvements of the MODIS Gross Primary Productivity Model Based on a Comprehensive Uncertainty Assessment over the Brazilian Amazonia. *ISPRS J. Photogramm. Remote Sens.* **2018**, *145*, 268–283. [[CrossRef](#)]
80. Nagai, S.; Saigusa, N.; Muraoka, H.; Nasahara, K.N. What makes the satellite-based EVI-GPP relationship unclear in a deciduous broad-leaved forest? *Ecol. Res.* **2010**, *25*, 359–365. [[CrossRef](#)]
81. Turner, D.P.; Ritts, W.D.; Cohen, W.B.; Gower, S.T.; Running, S.W.; Zhao, M.; Costa, M.H.; Kirschbaum, A.A.; Ham, J.M.; Saleska, S.R. Evaluation of MODIS NPP and GPP products across multiple biomes. *Remote Sens. Environ.* **2006**, *102*, 282–292. [[CrossRef](#)]
82. Wang, L.; Zhu, H.; Lin, A.; Zou, L.; Qin, W.; Du, Q. Evaluation of the Latest MODIS GPP Products across Multiple Biomes Using Global Eddy Covariance Flux Data. *Remote Sens.* **2017**, *9*, 418. [[CrossRef](#)]
83. Gilmanov, T.G.; Aires, L.; Barcza, Z.; Baron, V.S.; Belelli, L.; Beringer, J.; Billesbach, D.; Bonal, D.; Bradford, J.; Ceschia, E.; et al. Productivity, Respiration, and Light Response Parameters of World Grassland and Agroecosystems Derived from Flux Tower Measurements. *Rangel. Ecol. Manag.* **2010**, *63*, 16–39. [[CrossRef](#)]
84. Zhu, X.; Pei, Y.; Zheng, Z.; Dong, J.; Zhang, Y.; Wang, J.; Chen, L.; Doughty, R.; Zhang, G.; Xiao, X. Underestimates of Grassland Gross Primary Production in MODIS Standard Products. *Remote Sens.* **2018**, *10*, 1771. [[CrossRef](#)]
85. Wang, J.; Dong, J.; Liu, J.; Huang, M.; Li, G.; Running, S.W.; Smith, W.K.; Harris, W.; Saigusa, N.; Kondo, H.; et al. Comparison of gross primary productivity derived from GIMMS NDVI3g, GIMMS, and MODIS in southeast Asia. *Remote Sens.* **2014**, *6*, 2108–2133. [[CrossRef](#)]
86. Germano, M.F.; Vitorino, M.I.; Cohen, J.C.P.; Costa, G.B.; Souto, J.I.O.; Rebelo, M.T.C.; Sousa, A.M.L. Analysis of the breeze circulations in eastern Amazon: An observational study. *Atmos. Sci. Lett.* **2017**, *18*, 67–75. [[CrossRef](#)]
87. Zeri, M.; Sá, L.D.A. The Impact of Data Gaps and Quality Control Filtering on the Balances of Energy and Carbon for a Southwest Amazon Forest. *Agric. For. Meteorol.* **2010**, *150*, 1543–1552. [[CrossRef](#)]
88. Wutzler, T.; Lucas-Moffat, A.; Migliavacca, M.; Knauer, J.; Sickel, K.; Šigut, L.; Menzer, O.; Reichstein, M. Basic and Extensible Post-Processing of Eddy Covariance Flux Data with REddyProc. *Biogeosciences* **2018**, *15*, 5015–5030. [[CrossRef](#)]
89. Lucas-Moffat, A.M. Multiple Gap-Filling for Eddy Covariance Datasets. *Agric. For. Meteorol.* **2022**, *325*, 109114. [[CrossRef](#)]

**Disclaimer/Publisher’s Note:** The statements, opinions and data contained in all publications are solely those of the individual author(s) and contributor(s) and not of MDPI and/or the editor(s). MDPI and/or the editor(s) disclaim responsibility for any injury to people or property resulting from any ideas, methods, instructions or products referred to in the content.